

Invertible DenseNets with Concatenated LipSwish

Yura Perugachi-Diaz¹ Jakub M. Tomczak¹ Sandjai Bhulai¹

Abstract

We introduce Invertible Dense Networks (i-DenseNets), a more parameter efficient alternative to Residual Flows. The method relies on an analysis of the Lipschitz continuity of the concatenation in DenseNets, where we enforce invertibility of the network by satisfying the Lipschitz constant. We extend this method by proposing a learnable concatenation, which not only improves the model performance but also indicates the importance of the concatenated representation. Additionally, we introduce the Concatenated LipSwish as activation function, for which we show how to enforce the Lipschitz condition and which boosts performance. The new architecture, i-DenseNet, out-performs Residual Flow and other flow-based models on density estimation evaluated in bits per dimension, where we utilize an equal parameter budget. Moreover, we show that the proposed model out-performs Residual Flows when trained as a hybrid model where the model is both a generative and a discriminative model.

1. Introduction

Neural networks are widely used to parameterize non-linear models in supervised learning tasks such as classification. In addition, they are also utilized to build flexible density estimators of the true distribution of the observed data (MacKay & Gibbs, 1999; Rippel & Adams, 2013). The resulting deep density estimators, also called deep generative models, can be further used to generate realistic-looking images that are hard to separate from real ones, detection of adversarial attacks (Fetaya et al., 2019; Jacobsen et al., 2018), and for hybrid modeling (Nalisnick et al., 2019) which have the property to both predict a label (classify) and generate.

Many deep generative models are trained by maximizing the (log-)likelihood function and their architectures come in different designs. For instance, causal convolutional neural networks are used to parameterize autoregressive models

¹Vrije Universiteit Amsterdam, the Netherlands. Correspondence to: Yura Perugachi-Diaz <y.m.perugachidiaz@vu.nl>.

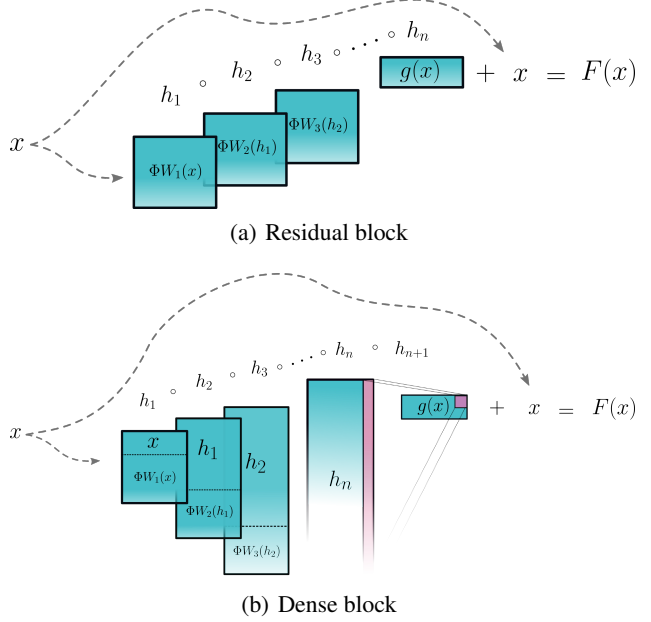


Figure 1. A schematic representation for: (a) a residual block, (b) a dense block.

(Oord et al., 2016a;b) or various neural networks can be utilized in Variational Auto-Encoders (Kingma & Welling, 2013; Rezende et al., 2014). The other group of likelihood-based deep density estimators, *flow-based models* (or *flows*), consist of invertible neural networks since they are used to compute the likelihood through the change of variable formula (Rezende & Mohamed, 2015; Tabak et al., 2010; Tabak & Turner, 2013). The main difference that determines an exact computation or approximation of the likelihood function for a flow-based model lies in the design of the transformation layer and tractability of the Jacobian-determinant. Many flow-based models formulate the transformation that is invertible and its Jacobian is tractable (Berg et al., 2018; De Cao et al., 2019; Dinh et al., 2015; Kingma et al., 2016; Papamakarios et al., 2017; Rezende & Mohamed, 2015; Tomczak & Welling, 2016). For example, in (Dinh et al., 2017) coupling layers are introduced that process only half of the input to calculate the Jacobian-determinant exactly. This allows the exact computation of both the inverse and the likelihood function.

Recently, Behrmann et al. (2019) proposed a different ap-

proach, namely, deep-residual blocks as a transformation layer. The deep-residual networks (ResNets) of (He et al., 2016) are known for their successes in supervised learning approaches. In a ResNet block, each input of the block is added to the output, which forms the input for the next block. Since ResNets are not necessarily invertible, Behrmann et al. (2019) enforce the Lipschitz constant of the transformation to be smaller than 1 (i.e., it becomes a contraction) that allows applying an iterative procedure to invert the network. Furthermore, Chen et al. (2019) proposed Residual Flows, an improvement of i-ResNets, that uses an unbiased estimator for the logarithm of the Jacobian-determinant.

In supervised learning, an architecture that uses fewer parameters and is even more powerful than the deep-residual network is the Densely Connected Convolution Network (DenseNet), which was first presented in (Huang et al., 2017). In contrary to a ResNet block, a DenseNet layer consists of a concatenation of the input with the output. The network showed to improve significantly in recognition tasks on benchmark datasets such as CIFAR10, SVHN, and ImageNet, by using fewer computations and having fewer parameters than ResNets while performing at a similar level.

In this work, we propose to extend Residual Flows (Behrmann et al., 2019; Chen et al., 2019), and replace the residual blocks with densely connected blocks (DenseBlocks). First, we introduce invertible Dense Networks (i-DenseNets), and we show that we can similarly enforce the Lipschitz constant as in (Behrmann et al., 2019) to create an invertible flow-based model. Furthermore, we propose the Concatenated LipSwish as an activation function, which is inspired by the Concatenated ReLU (Shang et al., 2016). We enforce it to satisfy the Lipschitz constant being strictly smaller than 1 and show how this activation function aids training more, compared to LipSwish. Finally, we demonstrate how i-DenseNets can be efficiently trained as a generative model, outperforming Residual Flows and other flow-based models under an equal parameter budget, where we focus on models using uniform dequantization.

2. Background

Flow-based models Let us consider a vector of observable variables $x \in \mathbb{R}^d$ and a vector of latent variables $z \in \mathbb{R}^d$. We define a bijective function $f : \mathbb{R}^d \rightarrow \mathbb{R}^d$ that maps a latent variable to a datapoint $x = f(z)$. Since f is invertible, we define its inverse as $F = f^{-1}$. We use the *change of variables formula* to compute the likelihood of a datapoint x after taking the logarithm, that is:

$$\ln p_X(x) = \ln p_Z(z) + \ln |\det J_F(x)|, \quad (1)$$

where $p_Z(z)$ is a base distribution (e.g., the standard Gaussian) and $J_F(x)$ is the Jacobian of F at x . The bijective transformation is typically constructed as a sequence of K

invertible transformations, $x = f_K \circ \dots \circ f_1(z)$, and a single transformation f_k is referred to as a *flow* (Rezende & Mohamed, 2015). The change of variables formula allows evaluating the data in a tractable manner. Moreover, the flows are trained using the log-likelihood objective where the Jacobian-determinant compensates the change of volume of the invertible transformations.

Uniform dequantization Flow-based models operate on continuous random variables. However, many objects take values in discrete domains, e.g., images are in $\{0, 1, \dots, 255\}^d$. In order to apply flows to images, we can utilize the *uniform dequantization* by adding a uniformly distributed noise $u \in [-0.5, 0.5]^d$ to the data, namely, $x = x_{org} + u$, where x_{org} is a vector of original pixel values. There are various schemes of dequantization (Hoogeboom et al., 2020a). Following (Behrmann et al., 2019), we use uniform dequantization (Theis et al., 2015).

Residual flows Behrmann et al. (2019) construct an invertible ResNet layer which is only constraint in Lipschitz continuity. A ResNet is defined as: $F(x) = x + g(x)$, where g is modeled by a (convolutional) neural network and F represents a ResNet layer (see Figure 1(a)) which is in general not invertible. However, g is constructed in such a way that it satisfies the Lipschitz constant being strictly lower than 1, $\text{Lip}(g) < 1$, by using spectral normalization of (Gouk et al., 2018; Miyato et al., 2018):

$$\text{Lip}(g) < 1, \quad \text{if} \quad \|W_i\|_2 < 1, \quad (2)$$

where $\|\cdot\|_2$ is the ℓ_2 matrix norm. Then $\text{Lip}(g) = K < 1$ and $\text{Lip}(F) \leq 1 + K$. Only in this specific case the Banach fixed-point theorem holds and ResNet layer F has a unique inverse. As a result, the inverse can be approximated by fixed-point iterations.

To estimate the log-determinant is, especially for high-dimensional spaces, computationally intractable due to expensive computations. Since ResNet blocks have a constrained Lipschitz constant, the log-likelihood estimation of Equation (1) can be transformed to a version where the logarithm of the Jacobian-determinant is cheaper to compute, tractable, and approximated with guaranteed convergence (Behrmann et al., 2019):

$$\ln p(x) = \ln p(f(x)) + \text{tr} \left(\sum_{k=1}^{\infty} \frac{(-1)^{k+1}}{k} [J_g(x)]^k \right), \quad (3)$$

where $J_g(x)$ is the Jacobian of g at x that satisfies $\|J_g\| < 1$. The Skilling-Hutchinson trace estimator (Skilling, 1989; Hutchinson, 1990) is used to compute the trace at a lower cost than to fully compute the trace of the Jacobian. Residual Flows (Chen et al., 2019) use an improved method to estimate the power series at an even lower cost with an

unbiased estimator based on "Russian roulette" of (Kahn, 1955). Intuitively, the method estimates the infinite sum of the power series by evaluating a finite amount of terms. In return, this leads to less computation of terms compared to invertible residual networks. To avoid derivative saturation, which occurs when the second derivative is zero in large regions, the LipSwish activation is proposed.

3. Invertible Dense Networks

In this section, we propose Invertible Dense Networks to parameterize a flow-based model. We refer to the resulting model as i-DenseNets. The code can be retrieved from https://github.com/yperugachidiaz/invertible_densenets.

3.1. Dense blocks

The main component of the proposed flow-based model is a DenseBlock that is defined as a function $F : \mathbb{R}^d \rightarrow \mathbb{R}^d$ with $F(x) = x + g(x)$, where g consists of dense layers $\{h_i\}_{i=1}^n$. A dense layer is expressed as follows:

$$g(x) = h_{n+1} \circ h_n \circ \dots \circ h_1(x), \quad (4)$$

where h_{n+1} represents a 1×1 convolution to match the output size of \mathbb{R}^d . A layer h_i consists of two parts concatenated to each other. The upper part is a copy of the input signal. The lower part consists of the transformed input, where the transformation is a multiplication of (convolutional) weights W_i with the input signal, followed by a non-linearity ϕ having $\text{Lip}(\phi) \leq 1$, such as ReLU, ELU, LipSwish, or tanh. As an example, a dense layer h_2 can be composed as follows:

$$h_1(x) = \begin{bmatrix} x \\ \phi(W_1 x) \end{bmatrix}, \quad h_2(h_1(x)) = \begin{bmatrix} h_1(x) \\ \phi(W_2 h_1(x)) \end{bmatrix}. \quad (5)$$

In Figure 1, we schematically outline a residual block (Figure 1(a)) and a dense block (Figure 1(b)).

3.2. Constraining the Lipschitz constant

If we enforce function g to satisfy $\text{Lip}(g) < 1$, then DenseBlock F is invertible since the Banach fixed point theorem holds. As a result, the inverse can be approximated in the same manner as in (Behrmann et al., 2019). To satisfy $\text{Lip}(g) < 1$, we need to enforce $\text{Lip}(h_i) < 1$ for all n layers, since the following holds: $\text{Lip}(g) \leq \text{Lip}(h_{n+1}) \cdot \dots \cdot \text{Lip}(h_1)$. Therefore, we first need to determine the Lipschitz constant for a dense layer h_i . We know that a function f is K -Lipschitz if for all points v and w the following holds (for the full derivation see Appendix A):

$$d_Y(f(v), f(w)) \leq K d_X(v, w), \quad (6)$$

where we assume that the distance metrics $d_X = d_Y = d$ are chosen to be the ℓ_2 -norm. Further, let two functions f_1

and f_2 be concatenated in h :

$$h_v = \begin{bmatrix} f_1(v) \\ f_2(v) \end{bmatrix}, \quad h_w = \begin{bmatrix} f_1(w) \\ f_2(w) \end{bmatrix}, \quad (7)$$

where function f_1 is the upper part and f_2 is the lower part. We can now find an analytical form to express a limit on K for the dense layer in the form of Equation (6):

$$\begin{aligned} d(h_v, h_w)^2 &= d(f_1(v), f_1(w))^2 + d(f_2(v), f_2(w))^2, \\ d(h_v, h_w)^2 &\leq (K_1^2 + K_2^2) d(v, w)^2, \end{aligned} \quad (8)$$

where we know that the Lipschitz constant of h consist of two parts, namely, $\text{Lip}(f_1) = K_1$ and $\text{Lip}(f_2) = K_2$. Therefore, the Lipschitz constant of layer h can be expressed as:

$$\text{Lip}(h) = \sqrt{K_1^2 + K_2^2}. \quad (9)$$

With spectral normalization of Equation (2), we know that we can enforce (convolutional) weights W_i to be at most 1-Lipschitz. Hence, for all n dense layers we apply the spectral normalization on the lower part which locally enforces $\text{Lip}(f_2) = K_2 < 1$. Further, since we enforce each layer h_i to be at most 1-Lipschitz and we start with h_1 , where $f_1(x) = x$, we know that $\text{Lip}(f_1) = 1$. Therefore, the Lipschitz constant of an entire layer can be at most $\text{Lip}(h) = \sqrt{1^2 + 1^2} = \sqrt{2}$, thus dividing by this limit enforces each layer to be at most 1-Lipschitz.

3.3. Learnable concatenation

We have shown that we can enforce an entire dense layer to have $\text{Lip}(h_i) < 1$ by applying a spectral norm on the (convolutional) weights W_i and then divide the layer h_i by $\sqrt{2}$. To optimize and learn the importance of the concatenated representations, we introduce learnable parameters η_1 and η_2 for, respectively, the upper and lower part of each layer h_i . Since the upper and lower part of the layer can be at most 1-Lipschitz, multiplication by these factors results in functions that are at most η_1 -Lipschitz and η_2 -Lipschitz. As indicated in the Appendix A, the layer is then at most $\sqrt{\eta_1^2 + \eta_2^2}$ -Lipschitz. Dividing by this factor results in a bound that is at most 1-Lipschitz.

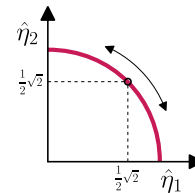


Figure 2. Range of the possible normalized parameters $\hat{\eta}_1$ and $\hat{\eta}_2$.

In practice, we initialize η_1 and η_2 at value 1 and during training use a softplus function to avoid them being negative. The range of the normalized parameters is between

$0 \leq \hat{\eta}_1, \hat{\eta}_2 \leq 1$ and can be expressed on the unit circle as shown in Figure 2. In the special case where $\eta_1 = \eta_2$, the normalized parameters are $\hat{\eta}_1 = \hat{\eta}_2 = \frac{1}{2}\sqrt{2}$. This case corresponds to the situation in Section 3.2 where the concatenation is not learned. An additional advantage is that the normalized $\hat{\eta}_1$ and $\hat{\eta}_2$ express the importance of the upper and lower signal. For example, when $\hat{\eta}_1 > \hat{\eta}_2$, the input signal is of more importance than the transformed signal.

3.4. CLipSwish

Residual Flows use the LipSwish activation function (Chen et al., 2019):

$$\text{LipSwish}(x) = x\sigma(\beta x)/1.1, \quad (10)$$

where $\sigma(\beta x) = 1/(1 + \exp(-x\beta))$ is the sigmoid. This activation function is not only $\text{Lip}(\text{LipSwish}) = 1$ but also resolves the derivative saturation problem (Chen et al., 2019). Since the gradients of the Jacobian depend on the second derivative, the derivative saturation problem arises when there are no or little second derivatives and is therefore difficult to optimize. Examples of this problem are the ELU and Softplus that obtain vanishing second derivatives when the derivative is maximal. LipSwish activation avoids this problem due to its construction.

Anil et al. (2019); Li et al. (2019) explain that 1-Lipschitz neural networks in practice have a Jacobian-norm that becomes much smaller than 1 which sacrifices expressive power, known as gradient norm attenuation. This problem arises in activation functions in regions where the derivative is small, such as the left tail of the ReLU and the LipSwish. Shang et al. (2016) proposed the Concatenated Rectified Linear Unit (CReLU). This activation function relies on a concatenation of the signal after a (convolutional) weight transformation, where signal x is concatenated with an exact copy of its negative signal $-x$, after which a ReLU is applied on both parts. The property of CReLU is that it has fewer problems with over-fitting compared to models using the regular ReLU. In Appendix A.2 we show how to derive the Lipschitz constant of the CReLU. However, the CReLU suffers from the derivative saturation problem.

Here, we propose the Concatenated LipSwish (CLipSwish). We will show how we can enforce the CLipSwish to be 1-Lipschitz in the upcoming derivation for a 1-dimensional input signal x .

We derive the upper bound of Concatenated LipSwish and we show that $\text{CLipSwish}(x) = \Phi(x)/1.004$ is enforced to satisfy $\text{Lip}(\text{CLipSwish}) = 1$. To start with, we define function $\Phi : \mathbb{R} \rightarrow \mathbb{R}^2$ for a point x as:

$$\Phi(x) = \begin{bmatrix} \phi_1(x) \\ \phi_2(x) \end{bmatrix} = \begin{bmatrix} \text{LipSwish}(x) \\ \text{LipSwish}(-x) \end{bmatrix}, \quad (11)$$

where the LipSwish is given by Equation (10) and the partial

derivative of $\Phi(x)$ exists. Then the Jacobian matrix of Φ is well-defined as:

$$J_\Phi(x) = \begin{bmatrix} \frac{\partial \phi_1(x)}{\partial x} \\ \frac{\partial \phi_2(x)}{\partial x} \end{bmatrix}. \quad (12)$$

Furthermore, we know that for a ℓ_2 -Lipschitz bounded function Φ , the following holds:

$$\text{Lip}(\Phi) = \sup_x \|J_\Phi(x)\|_2, \quad (13)$$

where $J_\Phi(x)$ is the Jacobian of Φ and norm $\|\cdot\|_2$ represents the induced matrix norm which is equal to the spectral norm of the matrix. Furthermore, we know that for a matrix A the following holds: $\|A\|_2 = \sigma_{\max}(A)$, where σ_{\max} is the largest singular value and the largest singular value is given by $\sigma_{\max}(A) = \sqrt{\lambda_1}$, since $\sigma_i = \sqrt{\lambda_i}$ for $i = 1, \dots, n$ (Lay, 2006). Now determining the singular values of $J_\Phi(x)$ is done by solving $\det(J_\Phi(x)^T J_\Phi(x) - \lambda I_n) = 0$. Combining and solving gives:

$$\begin{aligned} \det(J_\Phi(x)^T J_\Phi(x) - \lambda I_n) &= 0 \\ \left[\left(\frac{\partial \phi_1(x)}{\partial x} \right)^2 + \left(\frac{\partial \phi_2(x)}{\partial x} \right)^2 \right] - \lambda &= 0 \\ \lambda &= \left(\frac{\partial \phi_1(x)}{\partial x} \right)^2 + \left(\frac{\partial \phi_2(x)}{\partial x} \right)^2 \end{aligned} \quad (14)$$

where $\lambda = \lambda_1$ the largest eigenvalue, thus: $\lambda_1 = \left(\frac{\partial \phi_1(x)}{\partial x} \right)^2 + \left(\frac{\partial \phi_2(x)}{\partial x} \right)^2$. Therefore, the spectral norm of Equation (13), can be re-written as:

$$\begin{aligned} \|J_\Phi(x)\|_2 &= \sigma_{\max}(J_\Phi(x)) \\ &= \sqrt{\left(\frac{\partial \phi_1(x)}{\partial x} \right)^2 + \left(\frac{\partial \phi_2(x)}{\partial x} \right)^2}. \end{aligned} \quad (15)$$

Now $\text{Lip}(\Phi)$ is the upper bound of the CLipSwish and is equal to the supremum of: $\text{Lip}(\Phi) = \sup_x \|J_\Phi(x)\|_2 \approx 1.004$, for all values of β , which can be numerically computed by determining the extreme values. Therefore, dividing $\Phi(x)$ by its upper bound 1.004 results in $\text{Lip}(\text{CLipSwish}) = 1$. The generalization to higher dimensions can be found in Appendix A.3.

4. Experiments

To make a clear comparison between the performance of Residual Flows and i-DenseNets, we train both models on 2-dimensional toy data and high-dimensional image data: CIFAR10 and ImageNet32. Since we have a constrained computational budget, we use smaller architectures for the exploration of the network architectures. An in-depth analysis of different settings and experiments can be found in Section 5. Furthermore, for density estimation, we run the full

model with the best settings for 1,000 epochs on CIFAR10 and 20 epochs on ImageNet32. In all cases, we use the density estimation results of the Residual Flow and other flow-based models using uniform dequantization from (Chen et al., 2019) and benchmark these with i-DenseNets. We train i-DenseNets with LC and CLipSwish as the activation function, and utilize a similar number of parameters for i-DenseNets as Residual Flows; this can be found in Table 1. i-DenseNets uses slightly fewer parameters than the Residual Flow. A detailed description of the architectures can be found in Appendix B. To speed up training, we use 4 GPUs.

Table 1. The number of parameters of Residual Flows and i-DenseNets for the full models as trained in Chen et al. (2019). In brackets, the number of parameters of the smaller models.

Model/Data	CIFAR10	ImageNet32
Residual Flows	25.2M (8.7M)	47.1M
i-DenseNets	24.9M (8.7M)	47.0M

4.1. Toy data

We start with testing i-DenseNets and Residual Flows on toy data, where we use smaller architectures. Instead of 100 flow blocks, we use 10 flow blocks. We train both models for 50,000 iterations and, at the end of the training, we visualize the learned distributions.

The results of the learned density distributions are presented in Figure 3. We observe that Residual Flows are capable to capture high-probability areas. However, they have trouble with learning low probability regions for two circles and moons. i-DenseNets are capable of capturing all regions of the datasets. The good performance of i-DenseNets is also reflected in better performance in terms of the negative-log-likelihood (see Table 2).

Table 2. The negative log-likelihood results on test data in nats (toy data). i-DenseNets w/ and w/o learnable concatenation are compared with the Residual Flow.

Model	2 circles	checkerboard	2 moons
Residual Flows	3.44	3.81	2.60
i-DenseNets	3.32	3.68	2.39
i-DenseNets+LC	3.30	3.66	2.39

4.2. Density Estimation

We test the full i-DenseNet models with learnable concatenation and CLipSwish activation. To utilize a similar number of parameters as the Residual Flow with 3 scale levels and flow blocks set to 16 per scale trained on CIFAR10, we set for the same number of blocks, DenseNets growth to 172

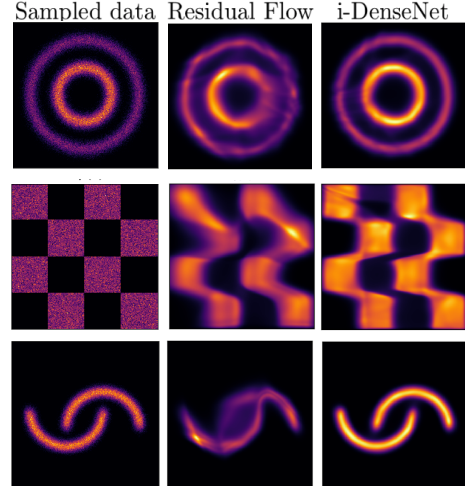


Figure 3. Images of density estimation for i-DenseNets trained on 2-dimensional toy data.

with a depth of 3. Residual Flow trained on ImageNet32 uses 3 scale levels with 32 flow blocks per scale, therefore, we set for the same number of blocks DenseNets growth to 172 and depth of 3 to utilize a similar number of parameters. DenseNets depth set to 3 proved to be the best settings for smaller architectures; see the analysis in Section 5.

The density estimation on CIFAR10 and ImageNet32 are benchmarked against the results of Residual Flows and other comparable flow-based models, where the results are retrieved from Chen et al. (2019). We measure performances in bits per dimension (bpd). The results can be found in Table 3. We find that i-DenseNets out-perform Residual Flows and other comparable flow-based models on all considered datasets in terms of bpd. On CIFAR10, i-DenseNet achieves 3.25bpd, against 3.28bpd of the Residual Flow. On ImageNet32 i-DenseNet achieves 3.98bpd against 4.01bpd of the Residual Flow. Samples of the i-DenseNet models can be found in Figure 4. Samples of the model trained on CIFAR10 are presented in Figure 4(b) and samples of the model trained on ImageNet32 in Figure 4(d). For more unconditional samples, see Appendix C.1.

Table 3. Density estimation results in bits per dimension for models using **uniform dequantization**. In brackets results for the smaller Residual Flow and i-DenseNet run for 200 epochs.

Model	CIFAR10	ImageNet32
Real NVP (Dinh et al., 2017)	3.49	4.28
Glow (Kingma & Dhariwal, 2018)	3.35	4.09
FFJORD (Grathwohl et al., 2019)	3.40	-
Flow++ (Ho et al., 2019)	3.29	-
ConvSNF (Hooeboom et al., 2020b)	3.29	-
i-ResNet (Behrmann et al., 2019)	3.45	-
Residual Flow (Chen et al., 2019)	3.28 (3.42)	4.01
i-DenseNet	3.25 (3.37)	3.98



Figure 4. Real and samples of CIFAR10 and ImageNet32 data

4.3. Uniform dequantization

This work does not compare against flow-based models using variational dequantization. Yet focuses on extending Residual Flows which, similarly to other flow-based models, use uniform dequantization. Note that Flow++ (Ho et al., 2019) with variational dequantization obtains 3.08bpd on CIFAR10 and 3.86bpd on ImageNet32 that is better than the same model with uniform dequantization (3.29bpd on CIFAR10).

4.4. Hybrid Modeling

Besides density estimation, we also experiment with hybrid modeling (Nalisnick et al., 2019). We train the joint distribution $p(\mathbf{x}, y) = p(\mathbf{x}) p(y|\mathbf{x})$, where $p(\mathbf{x})$ is modeled with a generative model and $p(y|\mathbf{x})$ is modeled with a classifier, which uses the features of the transformed image onto the latent space. Due to the different dimensionalities of y and \mathbf{x} , the emphasis of the likelihood objective is more likely to be focused on $p(\mathbf{x})$ and a scaling factor for a weighted maximum likelihood objective is suggested, $\mathbb{E}_{x, y \sim \mathcal{D}} [\log p(y|\mathbf{x}) + \lambda \log p(\mathbf{x})]$, where λ is the scaling factor expressing the trade-off between the generative and discriminative parts. Unlike (Nalisnick et al., 2019) where a linear layer is integrated on top of the latent representation, we use the architecture of (Chen et al., 2019) where the set of features are obtained after every scale level. Then, they are concatenated and are followed by a linear softmax classifier. We compare our experiments with the results of (Chen et al., 2019) where Residual Flow, coupling blocks (Dinh et al., 2015) and 1×1 convolutions (Kingma & Dhariwal, 2018) are evaluated.

Table 4 presents the hybrid modeling results on CIFAR10 where we used $\lambda = \{0, \frac{1}{D}, 1\}$. We run the three models for 400 epochs and note that the model with $\lambda = 1$ was not fully converged in both accuracy and bits per dimension after training. The classifier model obtains a converged accuracy after around 250 epochs. This is in line with the accuracy for the model with $\lambda = \frac{1}{D}$, yet based on bits

per dimension the model was not fully converged after 400 epochs. This indicates that even though the accuracy is not further improved, the model keeps optimizing the bits per dimension which gives room for future research. Results in Table 4 show the average result over the last 5 epochs. We find that Dense Blocks out-perform Residual Blocks for all possible λ settings. Interestingly, Dense Blocks have the biggest impact using no penalty ($\lambda = 1$) compared to the other models. We obtain an accuracy of 75.67% with 3.31bpd, compared to 70.32% accuracy and 3.39bpd of Residual Blocks, indicating that Dense Blocks significantly improves classification performance with more than 5%. In general, the Dense Block hybrid model is out-performing Real NVP, Glow, FFJORD, and i-ResNet in bits per dimension (see Appendix C.2 for samples of the hybrid models).

Table 4. Results of hybrid modeling on CIFAR10. Arrows indicate if low or high values are of importance. Results are average over the last 5 epochs.

Model \ Evaluation	$\lambda = 0$	$\lambda = \frac{1}{D}$		$\lambda = 1$	
	Acc \uparrow	Acc \uparrow	bpd \downarrow	Acc \uparrow	bpd \downarrow
Coupling	89.77%	87.58%	4.30	67.62%	3.54
+ 1×1 conv	90.82%	87.96%	4.09	67.38%	3.47
Residual Blocks (full)	91.78%	90.47%	3.62	70.32%	3.39
Dense Blocks (full)	92.40%	90.79%	3.49	75.67%	3.31

5. Analysis and Discussion

To get a better understanding of i-DenseNets, we perform additional experiments, explore different settings, analyze the results of the model and discuss future work. We use smaller architectures for these experiments due to a limited computational budget. For Residual Flows and i-DenseNets we use 3 scale levels set to 4 Flow blocks instead of 16 per scale level and train models on CIFAR10 for 200 epochs.

5.1. Activation Functions

We start with exploring different activation functions for both networks and test these with the smaller architectures. As (Chen et al., 2019) explained, an important property is

Table 5. Results in bits per dimensions for small architectures, testing different activation functions.

Model	LipSwish	LeakyLSwish	CLipSwish
Residual Flow	3.42	3.42	3.38
i-DenseNet	3.39	3.39	3.37

that an activation function ϕ should avoid derivative saturation by maintaining a second derivative, in order to avoid vanishing gradients. An activation function that is 1-Lipschitz and is a convex combination of an identity function and the LipSwish, is the LeakyLSwish, which allows freedom of movement in the left tail:

$$\text{LeakyLSwish}(x) = \alpha x + (1 - \alpha)\text{LipSwish}(x), \quad (16)$$

with $\alpha \in (0, 1)$ by passing it through a sigmoid function. We initialize the function at $\alpha = \sigma(-3)$ to mimic the LipSwish. Therefore, the three activation functions, LipSwish, LeakyLSwish, and CLipSwish, maintain the second derivative and, thus, maintain the signal, are tested. Note that the dimension for Residual Flows with CLipSwish activation function is set to 652 instead of 512 to maintain a similar number of parameters (8.7M) as with LipSwish activation.

Table 5 shows the results of each model using different activation functions. With 3.37bpd we conclude that i-DenseNet with CLipSwish as the activation function obtains the best performance compared to the other activation functions, LipSwish and LeakyLSwish. Furthermore, all i-DenseNets out-perform Residual Flows with the same activation function. We want to point out that CLipSwish as the activation function not only boosts performs of i-DenseNets but it also significantly improves the performance of Residual Flows whereas CLipSwish activation achieves 3.38bpd compared to the Residual Flow with 3.42bpd for LipSwish. This could be further deployed for future work.

Table 6. The mean and maximum ratio for different dimensions with sample size set to 100,000.

Activation \ Measure	$D = 1$		$D = 128$		$D = 1024$	
	Mean	Max	Mean	Max	Mean	Max
Sigmoid	0.22	0.25	0.21	0.22	0.21	0.21
LipSwish	0.46	1.0	0.51	0.64	0.51	0.55
CLipSwish	0.72	1.0	0.71	0.77	0.71	0.73
Identity	1.0	1.0	1.0	1.0	1.0	1.0

5.2. Analysis of activations and preservation of signals

When a deep neural network is bounded to be 1-Lipschitz, in practice each consecutive layer reduces the Jacobian-norm. As a result, the Jacobian-norm of the entire network is becoming much smaller than 1 and the expressive power is getting lost. This is known as *gradient norm attenuation*

(Anil et al., 2019; Li et al., 2019). Non-linearities ϕ modeled in i-DenseNets are required to be at most 1-Lipschitz and, thus, face gradient-norm attenuation issues. To analyze how much signal is preserved, we analyze the maximum and average distance ratios of sigmoid, LipSwish, and CLipSwish. Note that the maximum distance ratio approaches the Lipschitz constant and it is desired that the average distance ratio remains high.

We sample 100,000 datapoints $v, w \sim \mathcal{N}(0, 1)$ with dimension set to $D = \{1, 128, 1024\}$. We compute the mean and maximum of the sampled ratios with: $\ell_2(\phi(v), \phi(w)) / \ell_2(v, w)$ and analyze the expressive power of each function. Table 6 shows the results. We find that CLipSwish for all dimensions preserves most of the signal on average compared to the other non-linearities. This may explain why i-DenseNets with CLipSwish activation achieves better results than using, e.g., LipSwish.

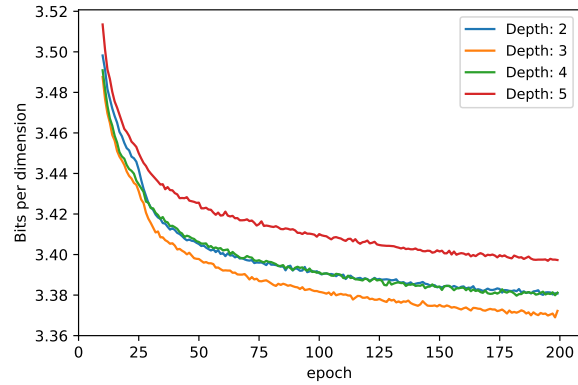


Figure 5. Effect of different concatenation depths with CLipSwish activation function for i-DenseNets in bits per dimension.

5.3. DenseNets concatenation depth

Next, we examine the effect of different concatenation depth settings for i-DenseNets. We run experiments with concatenation depth set to 2, 3, 4, and 5 with CLipSwish. Furthermore, to utilize 8.7M parameters of the Residual Flow, we choose a fixed depth and appropriate DenseNet growth size to have a similar number of parameters. This results in a DenseNet depth 2 with growth size 318 (8.8M), depth 3 with growth 178 (8.7M), depth 4 with growth 122 (8.7M), and depth 5 with growth 92 (8.8M). The effect of each architecture can be found in Figure 5. We observe that the model with a depth of 3 obtains the best scores and after 200 epochs it achieves the lowest bits per dimension with 3.37bpd. A concatenation depth of 5 results in 3.42bpd after 200 epochs, which is the least preferred. This could indicate that the corresponding DenseNet growth of 92 is too little to capture the density structure sufficiently and due to the deeper depth the network might lose important signals. Further, the figure clearly shows how learnable concatenation after 25 epochs boosts training for all i-DenseNets.

5.4. Importance of concatenated representation

Trained on CIFAR10, the smaller architecture with a DenseNet depth of 3, run for 200 epochs with CLipSwish obtains the best performance score with 3.37bpd. To analyze the importance of the concatenated representation after training, Figure 6 shows the heatmap for parameter $\hat{\eta}_1$ (Figure 6(a)) and parameter $\hat{\eta}_2$ (Figure 6(b)). Every scale level 1, 2, and 3 contains 4 DenseBlocks, that each contains 3 dense layers with convolutional layers. The final level FC indicates that fully connected layers are used. The letters ‘a’, ‘b’, and ‘c’ index the dense layers per block.

Remarkably, all scale levels for the last layers h_{ic} give little importance to the input signal. The input signals for these layers are in most cases multiplied with $\hat{\eta}_1$ (close to) zero, while the transformed signal uses almost all the information when multiplied with $\hat{\eta}_2$, which is close to one. This indicates that the transformed signal is of more importance for the network than the input signal. For the fully connected part, this difference is not that pronounced. Instead of 4 DenseBlocks, the full i-DenseNet model utilizes 16 DenseBlocks (CIFAR10) and 32 (ImageNet32) for every scale; these are not included due to the size.

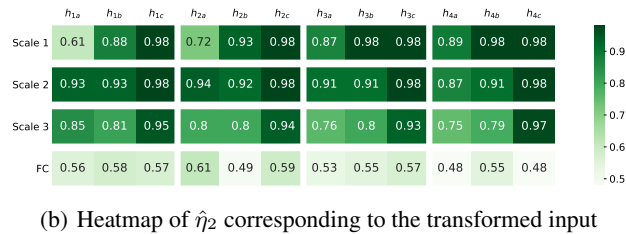
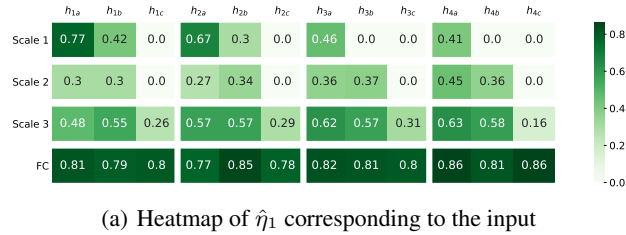


Figure 6. Heatmaps of the normalized η_1 and η_2 after training for 200 epochs on CIFAR10. Best viewed electronically.

5.5. Future Work

We introduced a new framework, i-DenseNet, that is inspired by Residual Flows and i-ResNets. We demonstrated how i-DenseNets out-performs Residual Flows and alternative flow-based models for density estimation and hybrid modeling, constraint by using uniform dequantization. For future work, we want to address several interesting aspects we came across and where i-DenseNets may be further deployed and explored.

First of all, we find that smaller architectures have more impact on performance than full models compared to Residual

Flows. Especially for exploration of the network, we recommend experimenting with smaller architectures or when a limited computational budget is available. This brings us to the second point. Due to a limited budget, we trained and tested i-DenseNets on 32×32 CIFAR10 and ImageNet32 data. It will be interesting to test higher resolution and other types of datasets.

Further exploration of DenseNets depth and growth for other or higher resolution datasets may be worthwhile. In our studies, deeper architectures did not result in better performance. However, it would also be beneficial to further examine the optimization of DenseNets architectures. Similarly, we showed how to constrain DenseBlocks for the ℓ_2 -norm. For future work, it may be interesting to generalize the method to different norm types, as well as the norm for CLipSwish activation function.

We want to stress that we focused on extending Residual Flows, which uses uniform dequantization. However, we believe that the performance of our network may be improved using variational dequantization or augmentation.

Finally, we found that especially hybrid model with $\lambda = 1$, achieve better performance than its predecessors. This may be worthwhile to further investigate in the future.

6. Conclusion

In this paper, we proposed i-DenseNets, a parameter-efficient alternative to Residual Flows. Our method enforces invertibility by satisfying the Lipschitz continuity in dense layers. In addition, we introduced a version where the concatenation of features is learned during training that indicates which representations are of importance for the model. Furthermore, we showed how to deploy the CLipSwish activation function. For both i-DenseNets and Residual Flows this significantly improves performance. Smaller architectures under an equal parameter budget were used for the exploration of different settings.

The full model for density estimation was trained on 32×32 CIFAR10 and ImageNet32 data. We demonstrated the performance of i-DenseNets and compared the models to Residual Flows and other comparable Flow-based models on density estimation in bits per dimension. Yet, it also demonstrated how the model could be deployed for hybrid modeling that includes classification in terms of accuracy and density estimation in bits per dimension. In conclusion, i-DenseNets out-perform Residual Flows and other competitive Flows-based models for density estimation on all considered datasets in bits per dimension and hybrid modeling that includes classification. The obtained results clearly indicate the high potential of i-DenseNets as powerful flow-based models.

Acknowledgements

We would like to thank Patrick Forré for his helpful feedback on the derivations. Furthermore, this work was carried out on the Dutch national e-infrastructure with the support of SURF Cooperative.

References

- Anil, C., Lucas, J., and Grosse, R. Sorting out lipschitz function approximation. In *International Conference on Machine Learning*, 2019.
- Behrmann, J., Grathwohl, W., Chen, R. T., Duvenaud, D., and Jacobsen, J.-H. Invertible residual networks. In *International Conference on Machine Learning*, 2019.
- Berg, R. v. d., Hasenclever, L., Tomczak, J. M., and Welling, M. Sylvester normalizing flows for variational inference. *arXiv preprint arXiv:1803.05649*, 2018.
- Chen, R. T. Q., Behrmann, J., Duvenaud, D., and Jacobsen, J. Residual flows for invertible generative modeling. In *Advances in Neural Information Processing Systems*, 2019.
- De Cao, N., Aziz, W., and Titov, I. Block neural autoregressive flow. In *Proceedings of the 35th Conference on Uncertainty in Artificial Intelligence*, 2019.
- Dinh, L., Krueger, D., and Bengio, Y. Nice: Non-linear independent components estimation. *arXiv:1410.8516*, 2015.
- Dinh, L., Sohl-Dickstein, J., and Bengio, S. Density estimation using real NVP. *arXiv:1605.08803*, 2017.
- Fetaya, E., Jacobsen, J.-H., Grathwohl, W., and Zemel, R. Understanding the limitations of conditional generative models. *arXiv:1906.01171*, 2019.
- Gouk, H., Frank, E., Pfahringer, B., and Cree, M. Regularisation of neural networks by enforcing Lipschitz continuity. *arXiv preprint arXiv:1804.04368*, 2018.
- Grathwohl, W., Chen, R. T. Q., Bettencourt, J., Sutskever, I., and Duvenaud, D. Ffjord: Free-form continuous dynamics for scalable reversible generative models. *International Conference on Learning Representations*, 2019.
- He, K., Zhang, X., Ren, S., and Sun, J. Deep residual learning for image recognition. In *Proceedings of the IEEE conference on computer vision and pattern recognition*, pp. 770–778, 2016.
- Ho, J., Chen, X., Srinivas, A., Duan, Y., and Abbeel, P. Flow++: Improving flow-based generative models with variational dequantization and architecture design. *arXiv preprint arXiv:1902.00275*, 2019.
- Hoogeboom, E., Cohen, T. S., and Tomczak, J. M. Learning discrete distributions by dequantization. *The 3rd Symposium on Advances in Approximate Bayesian Inference*, 2020a.
- Hoogeboom, E., Satorras, V. G., Tomczak, J. M., and Welling, M. The convolution exponential and generalized Sylvester flows. *arXiv preprint arXiv:2006.01910*, 2020b.
- Huang, G., Liu, Z., Van Der Maaten, L., and Weinberger, K. Q. Densely connected convolutional networks. In *IEEE Conference on Computer Vision and Pattern Recognition*, 2017.
- Hutchinson, M. F. A stochastic estimator of the trace of the influence matrix for laplacian smoothing splines. *Communications in Statistics-Simulation and Computation*, 19(2):433–450, 1990.
- Jacobsen, J.-H., Behrmann, J., Zemel, R., and Bethge, M. Excessive invariance causes adversarial vulnerability. *arXiv:1811.00401*, 2018.
- Kahn, H. Use of different Monte Carlo sampling techniques. *Proceedings of Symposium on Monte Carlo Methods*, 1955.
- Kingma, D. P. and Dhariwal, P. Glow: Generative flow with invertible 1x1 convolutions. In *Advances in Neural Information Processing Systems*, pp. 10215–10224, 2018.
- Kingma, D. P. and Welling, M. Auto-encoding variational Bayes. *arXiv preprint arXiv:1312.6114*, 2013.
- Kingma, D. P., Salimans, T., Jozefowicz, R., Chen, X., Sutskever, I., and Welling, M. Improved variational inference with inverse autoregressive flow. In *Advances in Neural Information Processing Systems*, pp. 4743–4751, 2016.
- Lay, D. C. *Linear Algebra and its Applications*. Pearson, 2006.
- Li, Q., Haque, S., Anil, C., Lucas, J., Grosse, R. B., and Jacobsen, J.-H. Preventing gradient attenuation in Lipschitz constrained convolutional networks. In *Advances in Neural Information Processing Systems*, pp. 15390–15402, 2019.
- MacKay, D. J. and Gibbs, M. N. Density networks. *Statistics and neural networks: advances at the interface*. Oxford University Press, Oxford, pp. 129–144, 1999.
- Miyato, T., Kataoka, T., Koyama, M., and Yoshida, Y. Spectral normalization for generative adversarial networks. *arXiv preprint arXiv:1802.05957*, 2018.

- Nalisnick, E., Matsukawa, A., Teh, Y. W., Gorur, D., and Lakshminarayanan, B. Hybrid Models with Deep and Invertible Features. In *International Conference on Machine Learning*, 2019.
- Oord, A. v. d., Dieleman, S., Zen, H., Simonyan, K., Vinyals, O., Graves, A., Kalchbrenner, N., Senior, A., and Kavukcuoglu, K. Wavenet: A generative model for raw audio. *arXiv preprint arXiv:1609.03499*, 2016a.
- Oord, A. v. d., Kalchbrenner, N., and Kavukcuoglu, K. Pixel recurrent neural networks. In *International Conference on Machine Learning*, pp. 1747–1756, 2016b.
- Papamakarios, G., Pavlakou, T., and Murray, I. Masked autoregressive flow for density estimation. In *Advances in Neural Information Processing Systems*, pp. 2338–2347, 2017.
- Rezende, D. J. and Mohamed, S. Variational inference with normalizing flows. *arXiv preprint arXiv:1505.05770*, 2015.
- Rezende, D. J., Mohamed, S., and Wierstra, D. Stochastic backpropagation and approximate inference in deep generative models. In *International Conference on Machine Learning*, 2014.
- Rippel, O. and Adams, R. P. High-dimensional probability estimation with deep density models. *arXiv preprint arXiv:1302.5125*, 2013.
- Shang, W., Sohn, K., Almeida, D., and Lee, H. Understanding and improving convolutional neural networks via concatenated rectified linear units. *arXiv:1603.05201*, 2016.
- Skilling, J. The eigenvalues of mega-dimensional matrices. In *Maximum Entropy and Bayesian Methods*, pp. 455–466. Springer, 1989.
- Tabak, E. G. and Turner, C. V. A family of nonparametric density estimation algorithms. *Communications on Pure and Applied Mathematics*, 66(2):145–164, 2013.
- Tabak, E. G., Vanden-Eijnden, E., et al. Density estimation by dual ascent of the log-likelihood. *Communications in Mathematical Sciences*, 8(1):217–233, 2010.
- Theis, L., Oord, A. v. d., and Bethge, M. A note on the evaluation of generative models. *arXiv preprint arXiv:1511.01844*, 2015.
- Tomczak, J. M. and Welling, M. Improving variational auto-encoders using householder flow. *arXiv preprint arXiv:1611.09630*, 2016.

A. Derivations

This appendix provides the reader full derivations of the Lipschitz constant for the concatenation in DenseNets and a bound of the Lipschitz for the activation functions.

A.1. Derivation of Lipschitz constant K for the concatenation

We know that a function f is K -Lipschitz if for all points v and w the following holds:

$$d_Y(f(v), f(w)) \leq K d_X(v, w), \quad (17)$$

where d_Y and d_X are distance metrics and K is the Lipschitz constant.

Consider the case where we assume to have the same distance metric $d_Y = d_X = d$, and where the distance metric is assumed to be chosen as any p -norm, where $p \geq 1$, for vectors: $\|\delta\|_p = \sqrt[p]{\sum_{i=1}^{len(\delta)} |\delta_i|^p}$. Further, we assume a DenseBlock to be a function h where the output for each data point v and w is expressed as follows:

$$h_v = \begin{bmatrix} f_1(v) \\ f_2(v) \end{bmatrix}, \quad h_w = \begin{bmatrix} f_1(w) \\ f_2(w) \end{bmatrix}, \quad (18)$$

where in this paper for a Dense Layer and for a data point x the function $f_1(x) = x$ and f_2 expresses a linear combination of (convolutional) weights with x followed by a non-linearity, for example $\phi(W_1 x)$. We can re-write Equation (17) for the DenseNet function as:

$$d(h_v, h_w) \leq K d(v, w), \quad (19)$$

where K is the unknown Lipschitz constant for the entire DenseBlock. However, we can find an analytical form to express a limit on K . To solve this, we know that the distance between h_v and h_w can be expressed by the p -norm as:

$$d(h_v, h_w) = \sqrt[p]{\sum_{i=1}^{len(h_v)} |h_{v,i} - h_{w,i}|^p}, \quad (20)$$

where we can simplify the equation by taking the p -th power:

$$d(h_v, h_w)^p = \sum_{i=1}^{len(f_1(v))} |f_1(v)_i - f_1(w)_i|^p + \sum_{i=1}^{len(f_2(v))} |f_2(v)_i - f_2(w)_i|^p. \quad (21)$$

Since we know that the distance of f_1 can be expressed as:

$$d(f_1(v), f_1(w)) = \sqrt[p]{\sum_{i=1}^{len(f_1(v))} |f_1(v)_i - f_1(w)_i|^p}, \quad (22)$$

which is similar for the distance of f_2 , re-writing the second term of Equation (21) in the form of Equation (19) is assumed to be of form:

$$d(f_1(v), f_1(w))^p \leq K_1^p d(v, w)^p, \quad (23)$$

which is similar for f_2 , $d(f_2(v), f_2(w))^p \leq K_2^p d(v, w)^p$. Assuming this, we can find a form of Equation (19) by substituting Equation (21) and Equation (23):

$$\begin{aligned} d(h_v, h_w)^p &= \sum_i^{len(h_v)} |h_{v,i} - h_{w,i}|^p \leq d(f_1(v), f_1(w))^p + d(f_2(v), f_2(w))^p \\ &= (K_1^p + K_2^p) d(v, w)^p. \end{aligned} \quad (24)$$

Now, taking the p -th root we have:

$$d(h_v, h_w) \leq \sqrt[p]{(K_1^p + K_2^p)d(v, w)}, \quad (25)$$

where we have derived the form of Equation (19) and where $\text{Lip}(h) = K$ is expressed as:

$$\text{Lip}(h) = \sqrt[p]{(K_1^p + K_2^p)}, \quad (26)$$

where $\text{Lip}(f_1) = K_1$ and $\text{Lip}(f_2) = K_2$, which are assumed to be known Lipschitz constants.

A.2. Derivation bounded Lipschitz Concatenated ReLU

We define function $\phi : \mathbb{R} \rightarrow \mathbb{R}^2$ as the Concatenated ReLU for a point x :

$$\phi(x) = \begin{bmatrix} \text{ReLU}(x) \\ \text{ReLU}(-x) \end{bmatrix}. \quad (27)$$

Let points $v, w \in \mathbb{R}$. From Section A.1, Equation (20), we know that the distance between points transformed with ϕ and using the ℓ_2 -norm can be written as:

$$\begin{aligned} d(\phi(v), \phi(w))^2 &= \sum_{i=1}^{\text{len}(\phi(v))} |\phi(v)_i - \phi(w)_i|^2 \\ &= (\phi(v)_1 - \phi(w)_1)^2 + (\phi(v)_2 - \phi(w)_2)^2 \\ &= (\text{ReLU}(v) - \text{ReLU}(w))^2 + (\text{ReLU}(-v) - \text{ReLU}(-w))^2. \end{aligned} \quad (28)$$

Furthermore, we know that the distance between the two points is:

$$\begin{aligned} d(v, w)^2 &= \sum_{i=1}^{\text{len}(v)} (v_i - w_i)^2 \\ &= (v - w)^2 \\ &= v^2 + w^2 - 2vw. \end{aligned} \quad (29)$$

We have four different situations that can happen. If $v > 0, w > 0$, then the distance between the points will be:

$$\begin{aligned} d(\phi(v), \phi(w))^2 &= (v - w)^2 + 0 \\ &= d(v, w)^2. \end{aligned} \quad (30)$$

In this specific case we have that $d(v, w)^2 = v^2 + w^2 - 2vw$, where $2vw > 0$. The same holds for $v \leq 0, w \leq 0$, when the first term becomes zero and instead of zero, the second term becomes $d(v, w)^2$ with $2vw \geq 0$.

If $v > 0, w \leq 0$, the distance between the points is equal to:

$$\begin{aligned} d(\phi(v), \phi(w))^2 &= (v - 0)^2 + (0 - w)^2 \\ &= v^2 + w^2 \\ &= (v - w)^2 + \underbrace{2vw}_{\leq 0} \leq (v - w)^2 = d(v, w)^2. \end{aligned} \quad (31)$$

The same derivation holds in the case $v \leq 0, w > 0$. Combining all cases, we find that $d(\phi(v), \phi(w)) \leq d(v, w)$, therefore:

$$\text{Lip}(\text{CReLU}) = 1. \quad (32)$$

A.3. Derivation Lipschitz bound of CLipSwish: Generalization to higher dimensions

To generalize the Concatenated LipSwish activation function to higher dimensions, we take $\Phi : \mathbb{R}^d \rightarrow \mathbb{R}^{2d}$, which represents the CLipSwish activation function for a vector $\mathbf{x} = \{x_1, x_2, \dots, x_d\}$. Then the CLipSwish is given by the concatenation $\Phi(\mathbf{x}) = [\text{LipSwish}(\mathbf{x}), \text{LipSwish}(-\mathbf{x})]$, where $\phi_1(\mathbf{x}) = \text{LipSwish}(\mathbf{x})$ and $\phi_2(\mathbf{x}) = \text{LipSwish}(-\mathbf{x})$ elementwise. The Jacobian matrix $J_\Phi(\mathbf{x})$ with shape $2d \times d$, looks as follows:

$$J_\Phi(\mathbf{x}) = \begin{bmatrix} \frac{\partial \phi_1(\mathbf{x})_1}{\partial x_1} & \frac{\partial \phi_1(\mathbf{x})_1}{\partial x_2} & \dots & \frac{\partial \phi_1(\mathbf{x})_1}{\partial x_d} \\ \vdots & \vdots & & \vdots \\ \frac{\partial \phi_1(\mathbf{x})_d}{\partial x_1} & \frac{\partial \phi_1(\mathbf{x})_d}{\partial x_2} & \dots & \frac{\partial \phi_1(\mathbf{x})_d}{\partial x_d} \\ \frac{\partial \phi_2(\mathbf{x})_1}{\partial x_1} & \frac{\partial \phi_2(\mathbf{x})_1}{\partial x_2} & \dots & \frac{\partial \phi_2(\mathbf{x})_1}{\partial x_d} \\ \vdots & \vdots & & \vdots \\ \frac{\partial \phi_2(\mathbf{x})_d}{\partial x_1} & \frac{\partial \phi_2(\mathbf{x})_d}{\partial x_2} & \dots & \frac{\partial \phi_2(\mathbf{x})_d}{\partial x_d} \end{bmatrix}, \quad (33)$$

where $\frac{\partial \phi_{i,j}}{\partial x_k} = \begin{cases} 0, & \text{if } j \neq k \\ \frac{\partial \phi_{i,j}}{\partial x_k}, & \text{otherwise.} \end{cases}$

The determinant is computed as $\det(J_\Phi(\mathbf{x})^T J_\Phi(\mathbf{x}) - \lambda I_n) = 0$, where $J_\Phi(\mathbf{x})^T J_\Phi(\mathbf{x})$ is of shape $d \times d$ with off-diagonals equal to zero. Therefore, the determinant is given by multiplication of the diagonal entries and each eigenvalue is given by each diagonal entry. The general form of determinant and eigenvalues is written as:

$$\det(J_\Phi(\mathbf{x})^T J_\Phi(\mathbf{x}) - \lambda I_n) = \prod_{j=1}^d \lambda_j, \quad (34)$$

where each eigenvalue is given by:

$$\lambda_j = \left(\frac{\partial \phi_{1,j}}{\partial x_j} \right)^2 + \left(\frac{\partial \phi_{2,j}}{\partial x_j} \right)^2. \quad (35)$$

Then:

$$\text{Lip}(\Phi) = \sup_x \|J_\Phi(x)\|_2 = \sup_x \max_j \sqrt{\lambda_j} = \sup_x \max_j \sqrt{\left(\frac{\partial \phi_{1,j}}{\partial x_j} \right)^2 + \left(\frac{\partial \phi_{2,j}}{\partial x_j} \right)^2} \approx 1.004, \quad (36)$$

where the last step is numerically approximated for the CLipSwish function, where ϕ is the LipSwish.

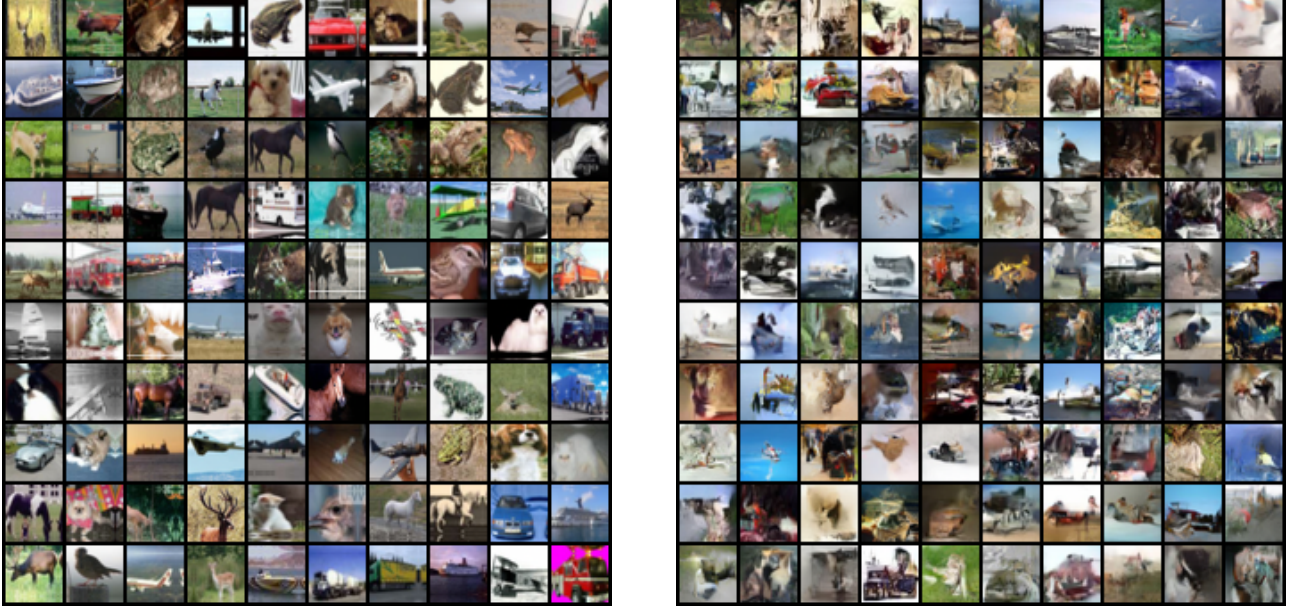
B. Implementation

During training we used a batch size of 64, CIFAR10 and ImageNet32 are of size 32×32 . Before training, uniform dequantization is applied to the images after which a logit transformation is applied. For hybrid models, instead of the logit transform, the images use normalization $x = \frac{x-\mu}{\sigma}$. As in (Chen et al., 2019), for evaluation at least 20 terms of the power series for the Jacobian-determinant are computed while the remaining terms to compute, are determined by the unbiased estimator. Furthermore, we set a bound on the Lipschitz constant of each dense layer with a Lipschitz coefficient of 0.98.

For all our models we ensured an equal parameter budget as the architecture of Residual Flows (Chen et al., 2019). For CIFAR10, the full i-DenseNets utilize 24.9M to utilize the 25.2M of Residual Flows. For ImageNet32, i-DenseNet utilizes 47.0M parameters to utilize the 47.1M of the Residual Flow. A numerical architecture of the full i-DenseNets for image data is presented in Table 7. A DenseBlock consists of several dense layers. The last dense layer h_n is followed by a 1×1 convolution to match the output of size \mathbb{R}^d , after which a squeezing layer is applied. The final part of the network consists of a Fully Connected (FC) layer with the number of blocks set to 4 for bot datasets. Before the concatenation in the FC layer, a Linear layer of input \mathbb{R}^d to output dimension 64 is applied, followed by the dense layer with for both datasets the FC DenseNet growth of 32, activation CLipSwish and a DenseNet depth of 3. The final part consists of a Linear layer to match the output of size \mathbb{R}^d . The large scale models require approximately 410 seconds for an epoch on 4 NVIDIA TITAN RTX GPUs.

Nr. of scales	Nr. of blocks per scale	DenseNet Depth	DenseNet Growth	Dense Layer	Output
3	16 (CIFAR10) 32 (ImageNet32)	3	172 (CIFAR10) 172 (ImageNet32)	$\begin{bmatrix} 3 \times 3 & \text{conv} \\ \text{CLipSwish} \\ \text{concat} \end{bmatrix}$	$\begin{bmatrix} 1 \times 1 & \text{conv} \end{bmatrix}$

Table 7. The general DenseNet architecture for the full models, modeled in function g for image data.



(a) Real images.

(b) Samples i-DenseNet.

Figure 7. Real images and samples from i-DenseNet trained on CIFAR10.

C. Samples

This appendix contains samples of the models trained on CIFAR10 and ImageNet32, along with samples of the hybrid models.

C.1. Model Samples

Figure 7 shows real images and samples of the models trained on CIFAR10. Figure 7(a) shows the real images and Figure 7(b) shows samples of i-DenseNet trained on CIFAR10.

Figure 8 contains real images and samples of the models trained on ImageNet32. Figure 8(a) shows the real images and Figure 8(b) shows samples of i-DenseNet trained on ImageNet32.

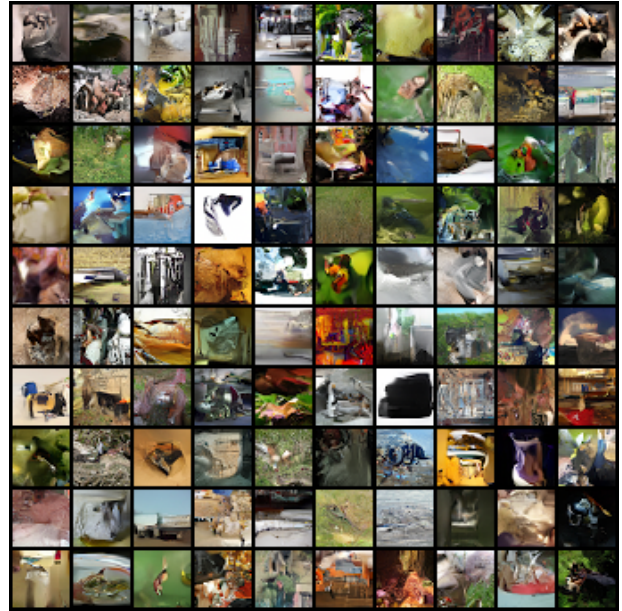
C.2. Hybrid modeling samples

Figure 9 shows samples of the hybrid models trained on CIFAR10. The model trained with a scaling factor of $\lambda = \frac{1}{D}$ can be found in Figure 9(a). We notice that the samples tend to show a lot of red and brown colors and that the images tend to look noisy. This is probably due to the scaling factor where the generative part and classifier part have an equal focus for the likelihood objective, while there are $D = 32 \times 32$ features per image.

The model trained with $\lambda = 1$ can be found in Figure 9(b). The samples tend to look like the samples in Figure 7(b), only with less definition. This is probably due to the extra part, namely, the classifier part. Comparing the bits per dimension of the hybrid model with i-DenseNet trained for density estimation only, we find a difference of 0.06bpd.



(a) Real images.

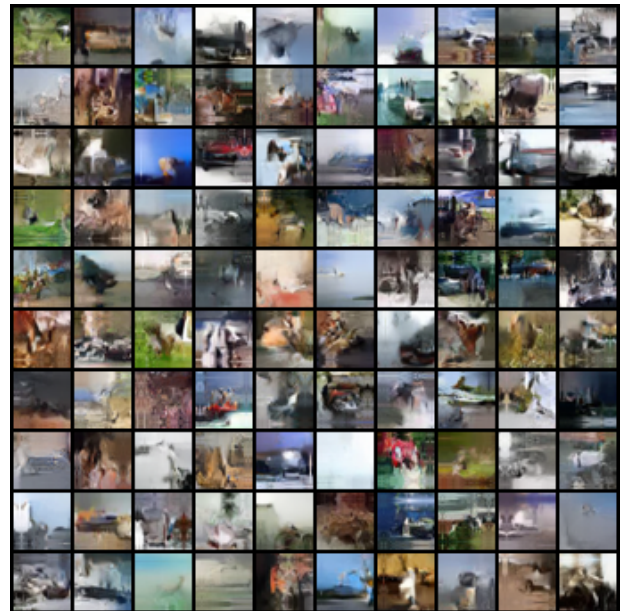


(b) Samples i-DenseNet.

Figure 8. Real images and samples from i-DenseNet trained on ImageNet32.



(a) Hybrid model trained with $\lambda = \frac{1}{D}$



(b) Hybrid model trained with $\lambda = 1$

Figure 9. Hybrid modeling results with Dense Blocks trained on CIFAR10